Experimental verification of super resolution in nonlinear inverse scattering

Fu-Chiarng Chen and Weng Cho Chew[a)]
Electromagnetics Laboratory, Center for Computational Electromagnetics, Department of Electrical and Computer Engineering, University of Illinois at Urbana-Champaign, Urbana, Illinois 61801

(Received 19 February 1998; accepted for publication 9 April 1998)

This letter presents an experimental verification of the super-resolution phenomenon in a nonlinear inverse scattering algorithm, namely the distorted Born iterative method, by using an experimental setup based on a recently developed time-domain ultra-wide-band radar imaging system at the University of Illinois at Urbana-Champaign. The experimental result also demonstrates that the distorted Born iterative method can recover information on the backside of a penetrable scatterer even though scattering data are collected only from limited viewing angles on the front side of the scatterer. © *1998 American Institute of Physics.* [S0003-6951(98)04423-4]

Super resolution refers to the resolution which is better than the Rayleigh resolution. Tomographic techniques can provide super resolution from a full viewing angle of target data collection. However, resolution tends to degrade to the Rayleigh resolution with the limited viewing angles data collection.[1] Spectral estimation is another method by which super resolution can be achieved.[2] The spectral estimation and tomographic techniques produce super resolution based on the spatial-frequency bandwidth. However, they do not take multiple scattering effects into account.

Recently, a nonlinear inverse scattering imaging algorithm, namely the distorted Born iterative method (DBIM), which accounts for both diffraction and multiple scattering effects has been developed.[3–5] DBIM is similar to the Newton-type method where the gradient of a nonlinear cost function is sought in order to minimize the cost function. Such a gradient method can be found by invoking a forward scattering solver. DBIM has been implemented for both cw and transient excitations. For the cw case, fast forward scattering solvers like the recursive aggregate T matrix algorithm (RATMA)[6] and CG-FFT method[7,8] can be used to reduce the computational time and memory requirement. For the transient case, a finite difference time domain (FDTD)[9] algorithm is used as the forward solver. In DBIM, the background medium is not constrained to be homogeneous and is updated at each iteration. DBIM has second-order convergence and hence is better for objects with large contrast.

The super-resolution phenomenon in nonlinear inverse scattering has been reported previously using numerically simulated data.[10,11] What was shown was the ability of a nonlinear inverse scattering method to resolve features that are much less than half a wavelength, the criterion dictated by the Rayleigh criterion. The phenomenon has been attributed to the multiple scattering effect within an inhomogeneous body. The high spatial frequency (high resolution) information of the object is usually contained in the evanescent waves when only single scattering physics is considered. Multiple scattering converts evanescent waves into propagating waves and vice versa. Hence, in an inverse scattering experiment, even though an object is interrogated with a propagating wave, and that only scattered waves corresponding to propagating waves can be measured, the scattered waves contain high resolution information about the scatterer because of the evanescent-propagating waves conversion in a multiply scattered field. Therefore, an inverse scattering method which unravels multiple scattering effects can extract the high resolution information on a scatterer.

The inverse scattering experimental setup is based on a time-domain ultra-wide-band radar imaging system recently developed at the University of Illinois at Urbana-Champaign.[12] Figure 1(a) shows the system block diagram of the system. The system consists of a Hewlett-Packard

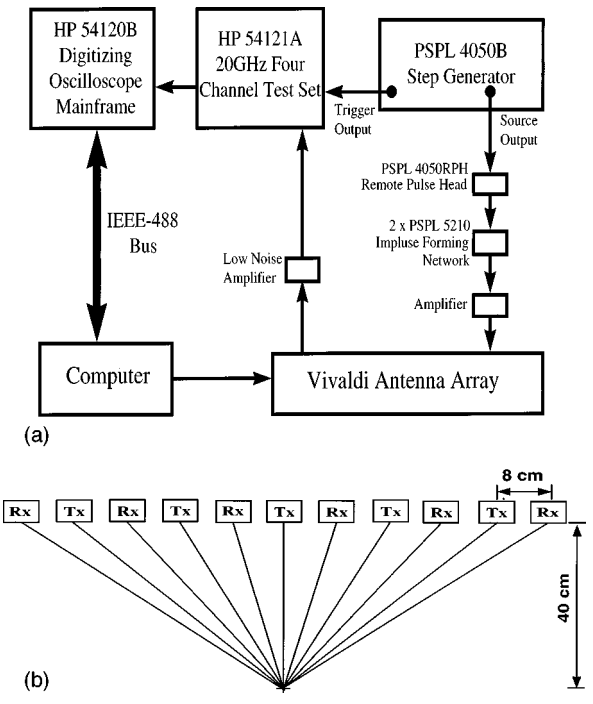

FIG. 1. (a) The time-domain ultra-wide-band imaging radar system blocks diagram. (b) The experimental setup of the switched Vivaldi antenna array. The eleven Vivaldi antennas are focused at the range of 40 cm.

a)Electronic mail: chew@sunchew.ece.uiuc.edu

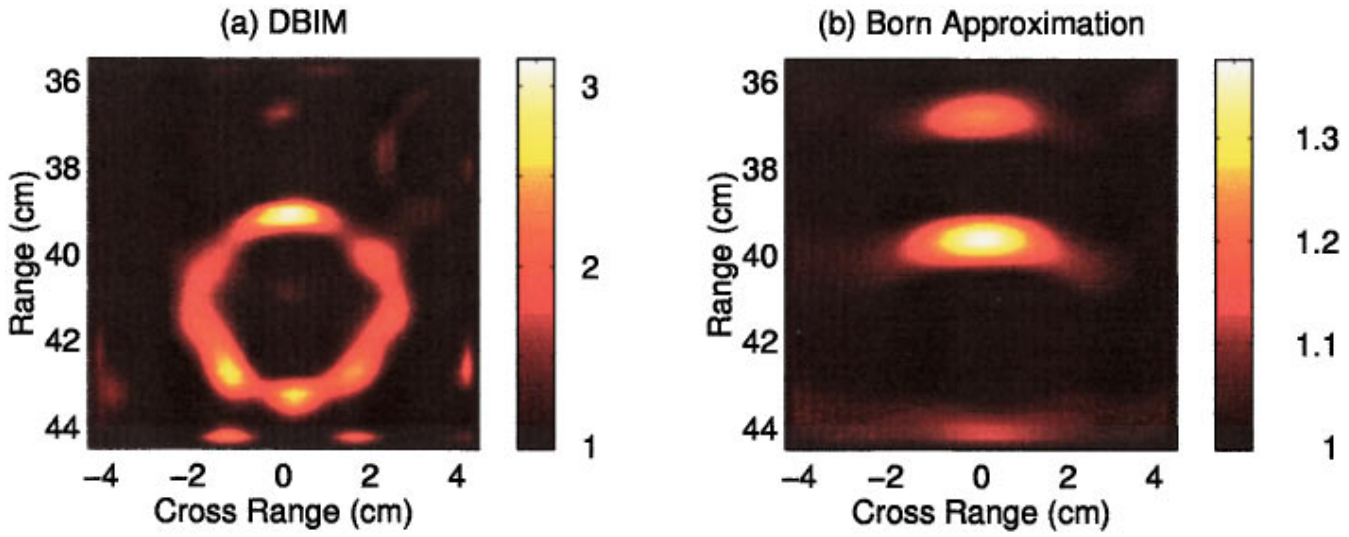

FIG. 2. (a) The DBIM permittivity reconstructed image of a plastic pipe (4.8 cm in outer diameter, 3.7 cm in inner diameter). (b) The reconstruction image of the same plastic pipe using the first-order Born approximation.

(HP) 54120B digitizing oscilloscope mainframe, an HP 54121A 20 GHz four-channel test set, a Picosecond Pulse Lab (PSPL) 4050B step generator, a PSPL 4050RPH remote pulse head, two PSPL 5210 impulse forming networks, a switched Vivaldi antenna[13,14] array, two ultra-wide-band amplifiers, and two microwave switches. The Vivaldi antenna array consists of five transmitting antennas and six receiving antennas. The Vivaldi antenna array is controlled by two microwave switches. The system is automated and controlled by a computer via the IEEE-488 bus.

A 10 V, 45 ps rise-time pulse is generated by the PSPL 4050B step generator with the PSPL 4050RPH remote pulse head. The timing jitter is only 1.5 ps rms. A 2.5 V, 50 ps impulse, and a 1.5 V, 10 GHz monocycle pulse are generated by attaching one or two PSPL 5210 impulse forming networks to the output of the 4050RPH remote pulse head. The monocycle pulse is chosen as the transmitting signal to match the operating bandwidth of the Vivaldi antenna array.

Figure 1(b) shows the experimental setup of the switched Vivaldi antenna array. The distance between the transmitting antenna and receiving antenna is 8 cm. All the 11 antennas of the array are focused at the range of 40 cm. The test scatterers are placed close to the focused zone. The distance between the scatterer and the antenna array is large enough so that only propagating waves are collected.

The collected 30 sets measurement data from the five transmitting and six receiving antennas in the switched Vivaldi antenna array are processed by DBIM to reconstruct the test scatterer.

Figure 2(a) shows the reconstructed image of a plastic pipe using DBIM permittivity reconstruction. The outer diameter of the plastic pipe is 4.8 cm. The inner diameter of the pipe is 3.7 cm. From the reconstruction result, the circular shape of the plastic pipe can be clearly observed and the reconstructed permittivity value of the plastic pipe is close to the actual value of 2.5. Figure 2(b) shows the reconstruction using first-order Born approximation. The reconstructed shape and the permittivity value are not correct because the Born approximation does not account for multiple scattering effect. The reconstruction results of Fig. 2 demonstrate that DBIM provides a much better result than the first-order Born approximation algorithm when multiple scattering phenomenon is significant.

The frequency spectrum of the scattered field from the plastic pipe is shown in Fig. 3(a). The half-wavelength corresponding to the frequency spectrum of the scattered field is shown in Fig. 3(b). From Fig. 3(a), it is seen that the scattered field is shown in Fig. 3(b). From Fig. 3(a), it is seen that the scattered field predominantly lies between 3 and 8 GHz. In addition, the magnitude of the spectrum at the high end frequency, 10 GHz, is about 40 dB lower than the peak value. From Figs. 2 and 3 we observe that DBIM achieves a 7.5 mm resolution which is better than quarter-wavelength for a high contrast scatterer. However, the first-order Born approximation reconstruction result is incorrect because it does not account for multiple scattering effects. In addition, the experiment demonstrates that DBIM can recover information on the backside of the scatterer even though scattering data are collected only from limited viewing angles on the front side of the scatterer. The reconstruction result also demonstrates that we are able to surpass the maximum contrast recovered by the first-order Born inversion[15] by a factor of about 25. Note that no *a priori* information about the object is needed in the reconstruction.

Figure 4(a) shows the reconstructed image of two plastic rods using DBIM permittivity reconstruction. The diameter of the plastic rods is 2 cm. The two rods are separated by 2.5 mm. This is much finer than the experimental setup's

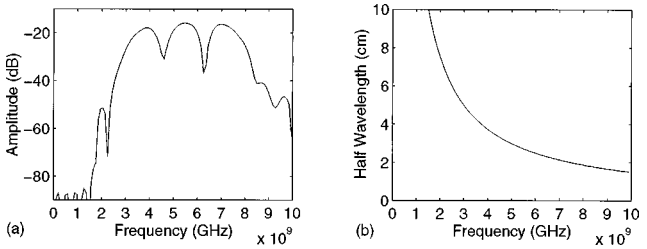

FIG. 3. (a) The frequency spectrum of the scattered field from the plastic pipe; (b) the half-wavelength corresponding to the frequency spectrum.

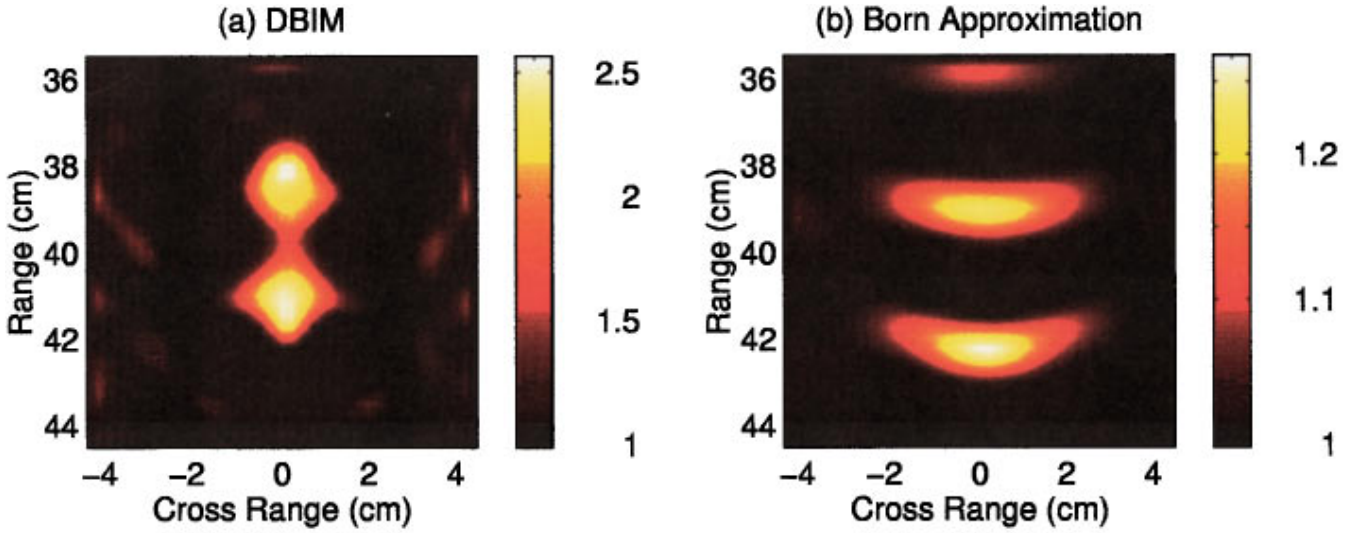

FIG. 4. (a) The DBIM permittivity reconstructed image of two plastic rods (2 cm in diameter, separated by 2.5 mm); (b) the reconstruction image of the same objects using the first-order Born approximation.

Rayleigh resolution of 1.5 cm for 10 GHz rf bandwidth or 1.875 cm for 8 GHz rf bandwidth. Figure 4(b) shows the reconstruction using first-order Born approximation. The reconstructed shape and the permittivity value are not correct because the Born approximation does not account for multiple scattering effect.

An experimental verification of the super-resolution phenomenon in nonlinear inverse scattering imaging is presented. The inverse scattering experimental setup is based on a recently developed time-domain ultra-wide-band.

[1] D. R. Wehner, *High-Resolution Radar* (Artech House, Norwood, MA, 1995).
[2] S. L. Marple, *Digital Spectral Analysis with Applications* (Prentice–Hall, Upper Saddle River, NJ, 1987), Chap. 8.
[3] Y.-M. Wang and W. C. Chew, Int. J. Imaging Syst. Technol. **1**, 100 (1989).
[4] W. C. Chew and Y. M. Wang, IEEE Trans. Med. Imaging **9**, 218 (1990).
[5] W. H. Weedon and W. C. Chew, *Review of Progress in Quantitative Nondestructive Evaluation* (Plenum, New York, 1997), Vol. 13, pp. 615–622.
[6] Y. M. Wang and W. C. Chew, Radio Sci. **27**, 109 (1992).
[7] D. T. Borup and O. P. Gandhi, IEEE Trans. Antennas Propag. **33**, 417 (1985).
[8] T. K. Sarkar, IEEE Trans. Antennas Propag. **34**, 635 (1986).
[9] K. S. Yee, IEEE Trans. Antennas Propag. **14**, 302 (1966).
[10] M. Moghaddam, W. C. Chew, and M. Oristaglio, Int. J. Imaging Syst. Technol. **3**, 318 (1991).
[11] M. Moghaddam and W. C. Chew, IEEE Trans. Geosci. Remote Sens. **GE-30**, 147 (1992).
[12] F.-C. Chen and W. C. Chew, *Review of Progress in Quantitative Nondestructive Evaluation* (Plenum, New York, 1997), Vol. 16, pp. 709–715.
[13] P. J. Gibson, in Proceedings of the Ninth European Microwave Conference, Brighton, UK, 1979, pp. 101–105.
[14] K. M. Frantz, M.S. thesis, University of Illinois at Urbana-Champaign, 1992.
[15] M. Slaney, A. C. Kak, and L. E. Larsen, IEEE Trans. Microwave Theory Tech. **32**, 860 (1984).